OpenFOAM® Journal

Volume 3 [16th OpenFOAM Workshop - 2021], Pages 146–158
ISSN: 2753-8168

Modelling Convective Heat Transfer of Air in a Data Center using OpenFOAM®- Evaluation of the Boussinesq Buoyancy Approximation

H. A. Barestrand[1,*], A-L. Ljung[1], J. Summers[1,2], and T. S. Lundström[1]

[1]Luleå University of Technology, division of fluid and experimental mechanics, Luleå, Sweden
Email address: henrik.barestrand@ltu.se, anna-lena.ljung@ltu.se, staffan.lundstrom@ltu.se

[2]RISE Research Institutes of Sweden, Luleå, Sweden
Email address: jon.summers@ri.se

DOI: https://doi.org/10.51560/ofj.v3.59
Results with version(s): OpenFOAM® v2012
Repository: -

Abstract. Achieving energy and cooling efficiency in data center convective air flow and heat transfer can be a challenging task. Among different numerical methods to work with such issues is the Finite Volume Method in Computational Fluid Dynamics. This work evaluates the performance of two such solvers provided by OpenFOAM®in solving this type of convective heat-transfer problem, namely *BuoyantBoussinesqPimpleFOAM* and *BuoyantPimpleFOAM*. This is done for two different flow configurations of significantly different Richardson number. To sufficiently resolve the flow, grid sizing effects are elucidated by way of the kernel density estimate. It determines the volume distribution of the temperature in the data center configuration. For the k-epsilon turbulence model used here, it was found that the compressible solver performs faster and requires less grid resolution for both flow configurations. This is attributed to the nature of the boundary conditions which are set such that the mass flow conservation per server rack and cooling unit is achieved. Transient solutions are found to provide better iterative convergence for cases that involves buoyancy, compressibility and flow separation. This is, in comparison to steady-state solutions where artificial numerical pressure drop is found, to depend on the momentum relaxation factors for the convective case with a higher Richardson number.

1. Introduction

The data center industry faces numerous challenges when it comes to cooling the equipment and distributing IT power and workload efficiently. An industry challenge today is to recover heat of the highest grade possible to enable process ecosystems that work in unison with the data centers. District heating and greenhouses are examples of this [1]. Different numerical tools and methods are therefore used to study heat transfer within data centers, ranging from Computational Fluid Dynamics (CFD) for the complexities of fluid flow to statistical and experimental models. The use of CFD in simulating feasible server load scenarios and its air convective effects beforehand yield information that in turn relates to the cooling performance [2]. This includes the processing of various metrics on whether the cold air in the data center is effectively delivered and also how the hot air is extracted [3].

Simulating the involved physics of airflow in a data center using the Finite Volume Method (FVM) is fairly complex and involves significant computational effort by today's standards. Faster methods for solving this type of problems have recently been developed based on the use of GPU's, though further work is deemed necessary to properly resolve the buoyancy, compressibility and wall effects along with turbulence modelling implementations [4].

When performing simulations of data centers a number of approximations are introduced on the geometry and boundary conditions. Such approximations often concern the simplification of geometry and how the racks are modelled. In this study focus is on the feasibility of which the Boussinesq approximation of buoyancy can be used when simulating this sort of convective heat transfer. The approximation is based on a linear expansion of the density in terms of temperature and has the potential to reduce the computational load for scenarios where there are limited temperature differences in the hot air. The

* Corresponding author

Received: 30 September 2021, Accepted: 13 October 2022, Published: 7 August 2023

approximation enables the use of an incompressible fluid solver along with a simplified energy equation in the FVM that disregards compressibility effects on the flow. The approximation has been shown to produce results within an error margin of 1% when temperature differences are below 15° C for air [5]. Expected temperature increase for air supplied to servers in data centers today are in an approximate range of 6-19° C [6], with an extended range if local temperatures inside the server racks near the power dissipation are considered.

The approximation itself requires some fluid quantities to be constant, namely μ, κ, α and c_p (viscosity, thermal conductivity, thermal diffusivity and specific heat). For numerical simulations of heating, ventilation and air conditioning, it is commonly assumed that one of these is constant. Thorough criteria along with an extensive analysis of the applicability of the Boussinesq approximation can be found in Tritton [7]. In this a brief summary is presented, focused on the question of whether forced or natural convection is dominating according to the Richardson number

$$\mathrm{Ri} = \frac{\mathrm{Gr}}{\mathrm{Re}^2} = \frac{g\nabla_z(\rho)}{\rho(\nabla_z(u))^2} \approx \frac{g\beta(T - T_{\mathrm{ref}})L_{\mathrm{vertical}}}{u^2} \tag{1}$$

where g denotes the gravitational constant, β is the thermal expansion coefficient and u is a typical velocity scale. For varying velocity scales in a complex flow, the Richardson number is more suitable than the Rayleigh number ($\mathrm{Ra} = \mathrm{Gr}\,\mathrm{Pr}$) to characterize the type of convection [7]. The limits: $\mathrm{Ri} \to 0$ and $\mathrm{Ri} \to \infty$ represent pure forced and pure natural convection, respectively. Transition between the flow regimes occurs at $\mathrm{Ri} \approx 0.3$ (from forced to mixed convection) and $\mathrm{Ri} \approx 16$ (from mixed to pure natural convection) [8].

For large Ri, turbulence is thought to take on characteristics other than what can be expected for small Ri. The length at which $\mathrm{Ri} = 1$ is called the Monin-Obukhov Length, which can here be seen as a reference height in determining stratification which in itself has a damping effect on turbulence [7].

The height at which cooling units supply air into data centers is often not more than a meter or so below where the hot air is returned. With previously mentioned temperatures and theorized limits for flow regimes the mixed flow regime can be predicted to reside in the velocity span $u \in (0.14, 1.83)$ m/s for a vertical length $L_{\mathrm{vertical}} = 1$ m, gravitational constant $g = 9.82$ m/s^2 and thermal expansion coefficient $\beta = 3.41 \times 10^{-3}$ K^{-1} based on Eqn. 1. Hence lowering the velocities in these areas can *in theory* enable significant stratification and in turn reduce wasteful mixing of hot and cold air.

In OpenFOAM terms, the solvers compared are *BuoyantBoussinesqPimpleFoam* and *BuoyantPimpleFoam*. The latter uses a compressible formulation for the pressure and implements a different form of the energy equation based on enthalpy. This difference in the energy equation includes a potential energy term on the right hand side, which at a higher Ri can be expected to significantly affect the solution. The Boussinesq and Compressible solvers mentioned here have both been previously validated toward indoor airflow applications [9].

1.1. **Research Aims.** This work builds upon previously demonstrated capability of OpenFOAM to simulate data center convection heat transfer by Summers et al. [10]. It is also to be a sound base for numerical studies of turbulence in data center open airflow situations connected to previous work by Wibron et al. [11]. In the earlier work by Wibron, a few different turbulence models were validated against measured flow data by the use of a hot wire anemometer. The limitations of the standard k-epsilon turbulence model was elucidated such that the near-wall flow and buoyant effects are not generally seen as well solved, though the results are still in general agreement for the statistically stationary flow [12].

To resolve data center airflow properly, the choice of turbulence model in conjunction with proper grid size and numerics is important. A study by Zhang et. al. found that results are not entirely grid independent, even for a grid resolution as fine as 1 inch per cell for data centers [13]. It is also found that results do not change significantly below a certain bulk cell size. To determine these requirements multiple grids are here used and compared.

Steady and transient solutions are also briefly compared, due to the transient nature of buoyancy, flow separation and compressibility. These are effects that can potentially put the RANS approach into jeopardy.

As for the modelling approach, the standard k-epsilon model has the advantage of being efficient, robust and frequently utilized for data center CFD modelling. Considering the caveats already mentioned, this model is chosen as it is known to generate solutions that exhibit statistically stationary flow. Unlike other Reynolds Averaged Navier Stokes (RANS) turbulence models, it exhibits a higher degree of stability and periodicity in the output temperatures on cooling units. It is therefore a model that is suited for this type of grid study. Meaning grid studies where long transient averages can otherwise be computationally

expensive to resolve. With the k-epsilon model, the flow can be averaged over a shorter period of time and then compared for the two solvers and cases.

This work also briefly concerns the procedure of verification, as there is no readily available data to validate the solution. With the main interest being the different results of the two solvers, a robust way of verification is desired. Richardson extrapolation is usually the preferred method for quantifying numerical errors [14]. Extrapolating a mean of a sampled variable during a set amount of time can however imply added errors, though it is not an uncommon thing to perform despite of said issue. Here a new qualitative approach is implemented to indicate the grid requirement necessary to obtain a solution in the asymptotic region of numerically resolved flow.

2. Method

The solvers are run and numerically verified for two different flow configurations. One where the Richardson number corresponds to a *typical* data center configutation and one where buoyant forces play a more prominent role in the flow. These numbers are calculated based on the resulting volume-averaged momentum for the two cases and presented as part of the results section. For the second(*reduced*) scenario, forced convection is reduced by lowering the mass flow rate through the modelled server racks and cooling units while retaining the heat generation. The Computer Room Air Handler (CRAH) flow rates are reduced to 1/5th of the *typical* mass along with all racks set to a uniform mass flowrate of 0.1 kg/s for the *reduced* case. These flow rates are presented in Tabs. 2 and 3. This is done to effectively test out the different solvers. This way it is possile to observe the effects of buoyancy by the heat distribution on the return side of different cooling units as well as the volume distribution of temperature.

The data center modelled here is part of the large scale data center research facility in Luleå, Sweden. Here a test module is used where various rack and cooling unit arrangements can be put together to find suitable configurations in terms of cooling performance and energy usage. This includes options of the hard floor and the more commonly used raised floor design. The hard floor configuration is chosen here to limit the added complexity of including floor tiles in the model.

Figure 1 shows the modelled data center, with dimensions being 6.50 x 7.00 x 3.15 m^3. The flow of air is such that a hot aisle in between the two rows of 5 racks each is formed. The hot air rises to the roof as a consequence of contributions from both forced and buoyant convection before returning to the cooling units.

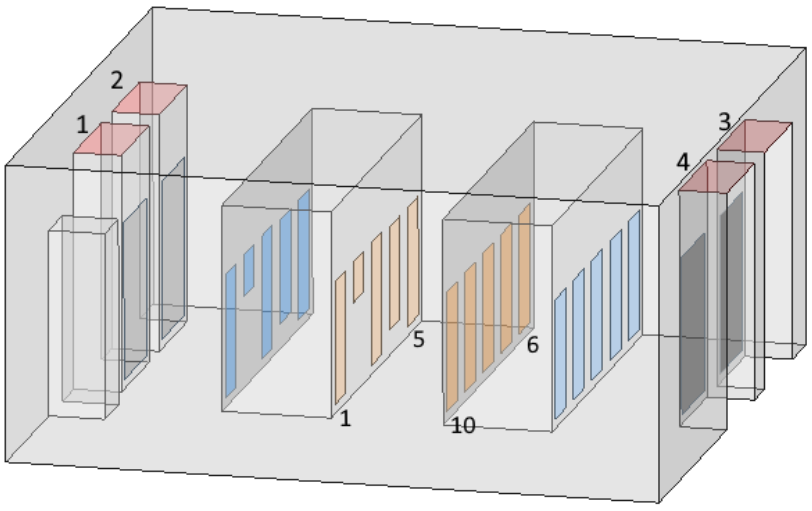

Figure 1. Model of the data center. Return areas of hot air to the CRAH are marked in red, near the roof. Supplied cool air enters the room through the gray areas and then flows through the servers, marked in blue and orange on the cold and hot side respectively

2.1. **Boundary Conditions & Numerics.** The solvers are both set up to use the same material properties (Tab. 1) and boundary conditions, with exception to the server enthalpy increase being dependent on the density of the incoming fluid for the compressible case.

The flow and heat generated from the servers is applied using the so called black-box model,

Table 1. Material properties

Property		Value	Unit
Laminar viscosity	ν	1.516e-5	$\mathrm{m}^2 \cdot \mathrm{s}^{-1}$
Reference density	ρ_0	1.205	$\mathrm{kg} \cdot \mathrm{m}^{-3}$
Specific heat	c_p	1006	$\mathrm{J} \cdot \mathrm{K}^{-1}$
Thermal expansion coefficient	β	3.43e-3	K^{-1}
Turbulent Prandtl number	Pr_t	0.85	
Laminar Prandtl number	Pr	0.707	

Table 2. Rack boundary conditions

Rack	Mass flow rate $\dot{m}$ (kg/s)	Heat load, P_{server} (W)
1	1.190	6208
2	0.605	3263
3	0.826	5458
4	0.438	3983
5	0.310	3463
6	0.353	4036
7	0.453	3982
8	0.240	2014
9	0.223	2057
10	0.243	2178

Table 3. Cooling unit boundary conditions

CRAH	Mass flow rate (kg/s)	Supply temperature, ($^\circ C$)
1	2.475	18.3
2	2.323	18.3
3	2.325	18.3
4	2.426	18.3

$$T_{\mathrm{in}} = T_{\mathrm{return}} + \frac{P_{\mathrm{rack}}}{\dot{m} c_p} \tag{2}$$

for server enthalpy increase [15]. Here the temperature increase is modelled as a function of rack power (P_{rack}) and mass flow ($\dot{m}$).

Supply temperatures, server loads and mass flow rates presented in Tabs. 2 and 3 depict the reference values used for the *typical* case, covering a realistic scenario for data center workloads and cold air supply [11]. Walls are set to be adiabatic along with the standard OpenFOAM®wall functions for k, ε and ν_t as *kLowReWallFunction*, *epsilonWallFunction* and *nutLowReWallFunction* respectively.

Various literature indicate static pressure openings for the CRAH-return boundaries should be used instead of specified mass flow outlet boundary conditions (possibly to improve numerical solution convergence) [11,16]. However, a specified static pressure affects the flow solution adversely such that consistent mass conservation per cooling unit is not imposed. An opening is therefore made in the geometry to act as a pressure reference to alleviate this, enabling the use of a specified flow rate for the CRAH-return areas.

For the transient simulations, the backward time iteration scheme is used along with second order discretization for velocity and temperature/energy. First order upwind discretization is used for the turbulence divergence terms, aiding significantly in convergence in comparison to second order schemes. No relaxation is used in the PISO-SIMPLE (PIMPLE) loop while 0.5 is set as default for velocity, energy and turbulence in the steady (SIMPLE) simulations. The SIMPLEC method is enabled for all cases to improve iterative convergence [17]. A maximum of 50 outer iterations are set, with two inner pressure corrections and one non-orthogonal correction deemed necessary for the snappyHexMesh generated grids.

The transient residual criteria are set to 1e-4 for all variables except for pressure with 1e-5 for each time step in the PISO-SIMPLE loop. The time step is set to be constant for all cases to dt=5e-3, resulting in Courant numbers of up to 3.3 for the finest grid for the *typical* case. In previous work by Wibron

et al. a larger time step of 5e-2 is possible due to the implicit equation coupling used in the element-based finite volume method [12]. An inherent assumption in using the RANS approach requires that a clear separation between turbulent and mean flow timescales are present, and that the time step used is greater than the turbulent time scales. The standard k-epsilon turbulence model for incompressible and compressible flows is used in this work, as included in OpenFOAM®v2012 excluding any added buoyant source terms.

Table 4. Definitions of the various numerical grids used for this study

Grid	Cells	Reference cell size, mm	Average edge length, mm
c	61.9k	140	123
n	88.8k	120	110
m	147k	100	92.9
f	282k	80	74.7
f_2	652k	60	56.5
f_3	1.12M	50	47.2
f_4	2.17M	40	37.8

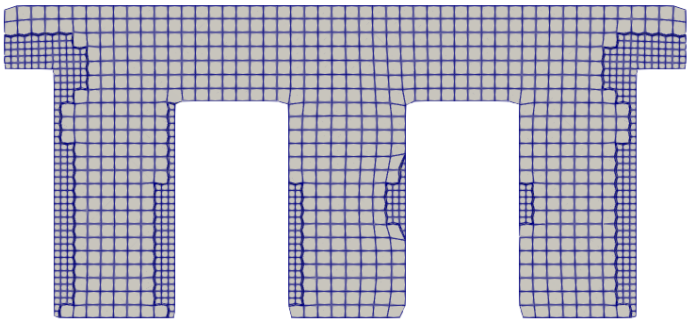

Figure 2. Slice cut of coarsest grid as generated by SnappyHexMesh (61.9k cells). The plane chosen intersects Racks 2 & 8 along with CRAH units 1 & 2 as viewed head on in Fig. 1

Seven different grids are used with sizes ranging from 40-140 mm for the Boussinesq case as seen in Tab. 4. Out of these grids, the finest solution is used to compare the solvers and cases. The grid generated by snappyHexMesh applies one refinement level beyond the initial uniform grid size near all flow boundaries as seen in Fig. 2. Refinement is applied near the racks to locally resolve temperature gradients and thus inhibit that numerical diffusion affects the downstream solution. With increased turbulence near the outlet boundaries the refinement region adds to solution accuracy here for the very same reason.

All cell temperature data is loaded and weighted by volume for an averaged transient solution span of 5 minutes to generate the histogram density plots. The method known as Kernel Density Estimation (KDE) for the temperature distribution in the volume is employed with a covariance factor that is optimized for the coarser grid [18]. The reason for using the covariance factor suited to the coarsest grid, when making the distribution plots, is that the temperature distributions under the same statistical frame can be compared.

2.2. **Governing Equations.** Here, the differential equations governing the fluid flow for the transient solvers are presented. These equations model the momentum, mass and energy conservation together with the turbulent viscosity ν_t based on the closure model selected. Compressibility is also an aspect of the turbulence model, which uses a convective formulation that includes density that may also affect the results.

2.2.1. *BuoyantBouissinesqPimpleFoam.* The Boussinesq solver employs a fully incompressible formulation where buoyancy is modelled as dependent on temperature, which in turn simplifies the energy equation to its constituents of pure convection and effective diffusion of temperature. The buoyant contribution to dynamic pressure is formulated such that the force added is linearly dependent on the temperature. The core equations for the Boussinesq solver includes continuity,

$$\boldsymbol{\phi} = \mathbf{u} \tag{3}$$
$$\nabla \cdot \boldsymbol{\phi} = 0 \tag{4}$$

and momentum,

$$D(\mathbf{u}) = \nabla\mathbf{u} + (\nabla\mathbf{u})^T \tag{5}$$
$$\frac{\partial \mathbf{u}}{\partial t} + \nabla \cdot (\boldsymbol{\phi}\mathbf{u}) - \nabla \cdot (\nu_{\text{eff}} D(\mathbf{u})) = -\frac{1}{\rho_0}(\nabla p_s - \rho\boldsymbol{g}) \tag{6}$$
$$= -\nabla p_{\text{rgh}} - (\mathbf{g} \cdot \mathbf{r})\nabla\rho_k \tag{7}$$

that is of the incompressible form where the dynamic pressure p_{rgh} includes the buoyant contribution. The kinematic pressure is specified for the incompressible solver based on the static pressure as $p_k = p_s/\rho_0$,

$$p_{\text{rgh}} = (p_k - \rho_k \mathbf{g} \cdot \mathbf{r}) \tag{8}$$
$$\rho_k = \frac{\rho}{\rho_0} = 1 - \beta(T - T_{\text{ref}}) \tag{9}$$
$$\tag{10}$$

with β as the coefficient of thermal expansion. The energy equation,

$$\frac{\partial \mathrm{T}}{\partial t} + \nabla \cdot (\boldsymbol{\phi}\mathrm{T}) - \alpha_{\text{eff}}\nabla^2\mathrm{T} = 0 \tag{11}$$
$$\alpha_{\text{eff}} = \frac{\nu}{\text{Pr}} + \frac{\nu_t}{\text{Pr}_t} \tag{12}$$

is modelled on the form of temperature as a transported scalar with diffusion by the turbulence.

2.2.2. *BuoyantPimpleFoam.* The compressible pressure based solver is defined such that continuity,

$$\boldsymbol{\phi} = \rho\mathbf{u} \tag{13}$$
$$\frac{\partial \rho}{\partial t} + \nabla \cdot \phi = 0 \tag{14}$$

and momentum,

$$D(\mathbf{u}) = \nabla\mathbf{u} + (\nabla\mathbf{u})^T - \frac{2}{3}(\nabla \cdot \mathbf{u})\mathbf{I} \tag{15}$$
$$\frac{\partial(\rho\mathbf{u})}{\partial t} + \nabla \cdot (\boldsymbol{\phi}\mathbf{u}) - \nabla \cdot (\rho\nu_{\text{eff}} D(\mathbf{u})) = -\nabla p_s + \rho\boldsymbol{g} \tag{16}$$
$$= -\nabla p_{\text{rgh}} - (\mathbf{g} \cdot \mathbf{r})\nabla\rho \tag{17}$$

computation is dependent on the ideal gas equation of state for the density.

$$\rho = \frac{p_s}{RT} \tag{18}$$
$$p_{\text{rgh}} = (p_s - \rho\mathbf{g} \cdot \mathbf{r}) \tag{19}$$

which adds complexity to the energy equation,

$$\frac{\partial}{\partial t}(\rho h) + \nabla \cdot [\phi h] - \cancelto{\text{off}}{\frac{\partial p}{\partial t}} - \nabla \cdot (\alpha_{\text{eff}}\nabla h) = \rho(\mathbf{g} \cdot \mathbf{u}) \tag{20}$$
$$\alpha_{\text{eff}} = \frac{\rho\nu_t}{\text{Pr}_t} + \frac{\mu}{\text{Pr}} \tag{21}$$

in the form on a potential energy term, $\rho(\mathbf{g} \cdot \mathbf{u})$. Specific enthalpy $h = \hat{u} + p/\rho$ is used with its internal energy $\hat{u}$ and constant specific heat c_p, such that essentially the temperature is evaluated by $h = c_p T$ and used to correct ρ before solving the energy for the next iteration. Also the pressure work term in Eqn. 20 is disabled for improved convergence in the simulations, since statistically stationary turbulent flow is considered.

The effective viscosity is again the superposition of turbulent and laminar viscosities($\nu_{\text{eff}} = \nu + \nu_t$) and with corresponding, constant Prandtl numbers (Pr, Pr_t) for the heat diffusivity.

3. Results & Discussion

An overview of the different simulations run in this work are displayed in Tab. 5 together with resulting normalized wall distance y^+. The results are presented in four sections, starting with the influence of the grid on the two flow rates chosen for the Boussinesq solver. The next two sections covers the solver influence for each scenario along with the steady and transient solution methods. Finally the scenarios are compared using the compressible solution for the finest grid. This includes a brief analysis of how the flow features exhibit significant differences when the Richardson number is changed.

With y^+ values lower than 30 for the natural convection case, the applied hybrid low reynolds wall model solution is considered applicable for the purpose of comparing the two solvers. Though in general, cell wall distances in ranges of the log-layer are desirable. It is also seen in Tab. 5 that the Boussinesq and Compressible cases are consistent to at least two digits in terms of the resulting wall distances.

Table 5. Simulation matrix

	Case		Grids	Average wall y^+
Boussinesq	$\mathrm{Ri}_{\mathrm{typical}}$	Steady	f_4	27.3
		Transient	**c**, n, m, **f**, f_2, f_3, $\mathbf{f_4}$	48.4 → 37.1 → 27.3
	$\mathrm{Ri}_{\mathrm{reduced}}$	Steady	f_4	15.7
		Transient	**c**, n, m, **f**, f_2, f_3, $\mathbf{f_4}$	27.9 → 21.9 → 15.7
Compressible	$\mathrm{Ri}_{\mathrm{typical}}$	Steady	f_4	27.3
		Transient	**f**, f_2, f_3, $\mathbf{f_4}$	37.1 → 27.3
		Startup	f_2	33.7
	$\mathrm{Ri}_{\mathrm{reduced}}$	Steady	f_4	15.7
		Transient	f_4	15.5
		Startup	f_2	19.3

3.1. **Grid comparisons.** The distribution of temperature in the entire data center volume in Fig. 3 shows the grid influence on the solution. Numerical diffusion is seen to occur for grids "c", "n" & "m" where volume is shifted to the intermediate temperature range inside the data center. It can also be seen that the three finest grids overlap their volume distribution to a high degree such that the solutions can be considered identical. This is further emphasized by the trends for the mean return temperatures and pressures presented in Figs. 4 and 5. With a cold side CRAH-temperature at 291.45 K, the 5-minutes sampled mean for the return sides seen in Fig. 4 differ by a maximum of .5 K for all grids. The pressure drop per cooling unit cold and hot side is seen in Fig. 5 to have differences of up to 1.5 Pa. These intervals are reduced for the three finest grids to .18 K and .3 Pa for the temperatures and pressure drops respectively. Pressure can thus be considered a more sensitive variable in regards to the quality of the solution as it closer relates to the the diffusion of temperature when comparing Figs. 5 and 3.

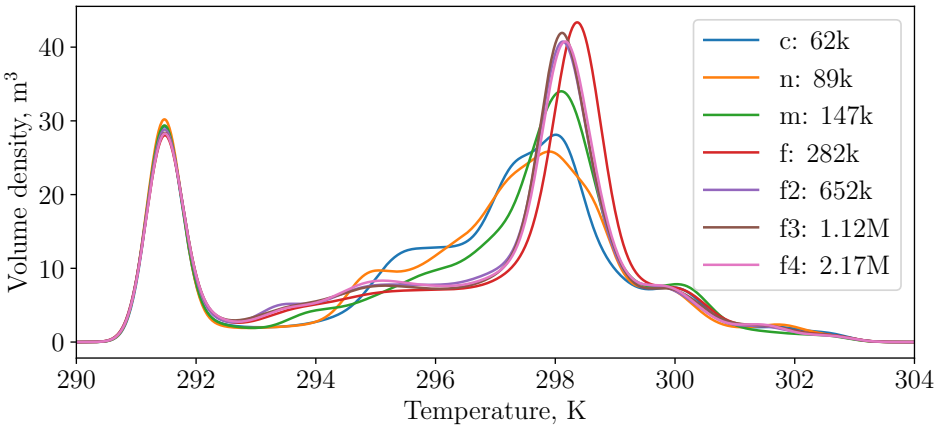

Figure 3. Volume distributions of temperature for the *typical* Boussinesq case with covariance factor of 0.1

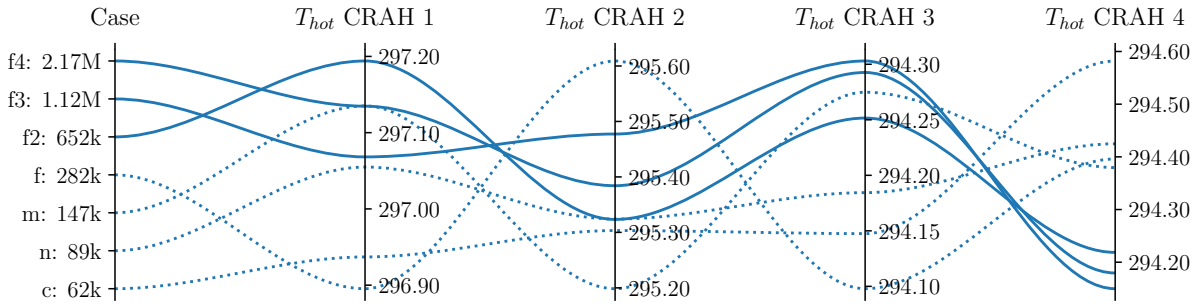

Figure 4. Return temperatures in K for the *typical* transient Boussinesq case with varied grid size

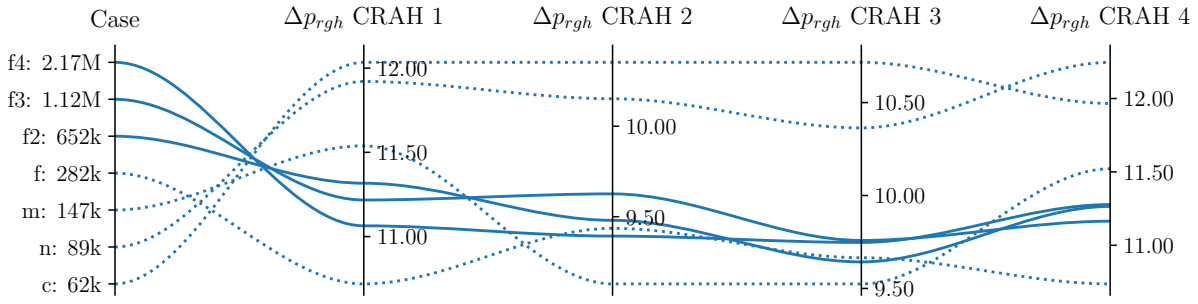

Figure 5. CRAH-unit pressure drops in Pa for the *typical* transient Boussinesq case with varied grid size

As for grid convergence, no extrapolation is performed in this work as we are looking for tendencial differences of the solutions between the solvers. Here focus is directed toward what type of grid densities to employ. Although five minutes sampled time is considered enough for obtaining a statistically steady solution for the k-epsilon model, extrapolation based on mean variables would need to deal with accompanying variances to determine that the solution is spatially resolved. Securing that the solution is in the asymptotic range of convergence is usually done with Richardson extrapolation. For transient cases the sampling has to be carried out for a significant time to have consistent extrapolated values as the extrapolation can be a very sensitive measure.

The convergence between grids for the compressible case is shown in Fig. 6, where there is no shift of the peak of highest temperature such as is seen for the "f" grid in Fig. 3. The Boussinesq solver thus likely has a finer grid requirement than the compressible solver for the *typical* scenario. The distributions in Figs. 3, 6 and 7 are generated as Kernel Density Estimations by use of constant covariance factors based on the coarsest grid presented in each figure. The estimation for the *reduced* flow rate case is seen in Fig. 7 where just slight distribution differences can be distinguished on the higher end of temperatures and again the three finest grids overlap. Errors introduced by varied cell wall distance may also contribute to the small differences. These results indicate that a reduced flow rate also implies a reduction in the grid requirement.

3.2. **Evaluation of solvers and a steady steate assumption for the *Typical* operation case.** Quantifying the mean temperature differences between the solvers (Boussinesq and compressible) for the three finest grids results in CRAH-return variations of up to 0.1 K. The compressible solver has a consistently larger pressure drop for all three fine grids in the range of 0.2 Pa for the cooling units. Pressure transients vary in the order of 0.1 Pa.

The steady-state solutions are measured to have similar mean return temperatures as the unsteady solutions to within 0.1 K for the cases presented in Fig. 8. Some minimal differences are found in the KDE distributions of turbulent kinetic energy for these solutions, indicating that the steady solutions have more kinetic energy. The increased pressure is attributed to artificial pressure arising in the numerics when relaxation is introduced. Added relaxation in a steady solution reduces the residuals and enables added steadiness. The two solvers are seen to respond similarly to the different cases with the compressible case resolving slightly more pressure drop.

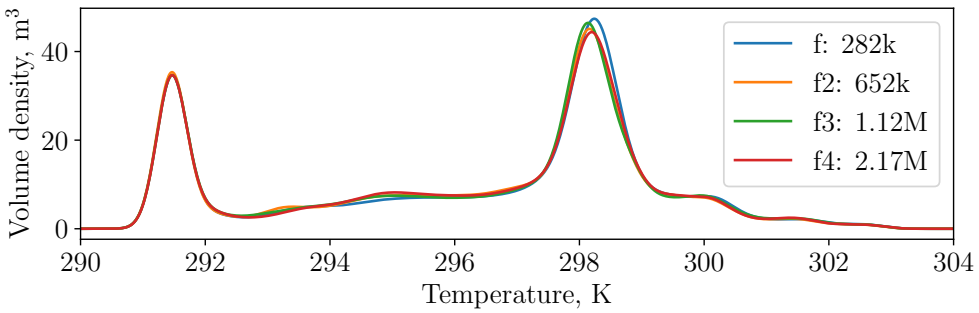

Figure 6. Settling of temperature diffusion with grid refinement for the *typical* compressible case with a covariance factor of 0.1

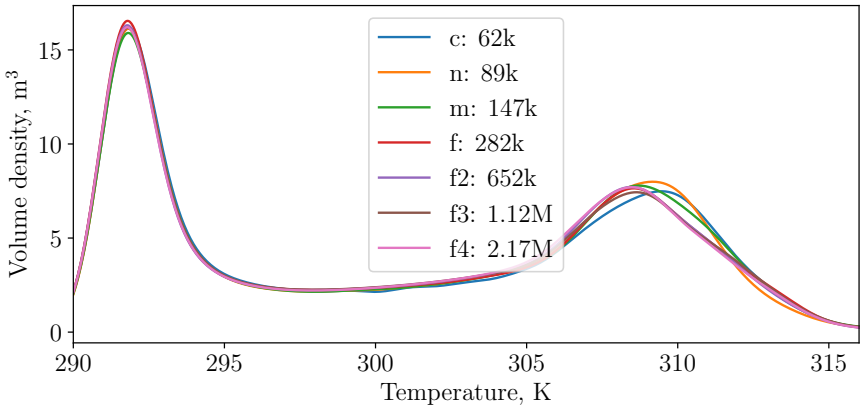

Figure 7. Temperature distribution due to grid differences for the *reduced* Boussinesq case

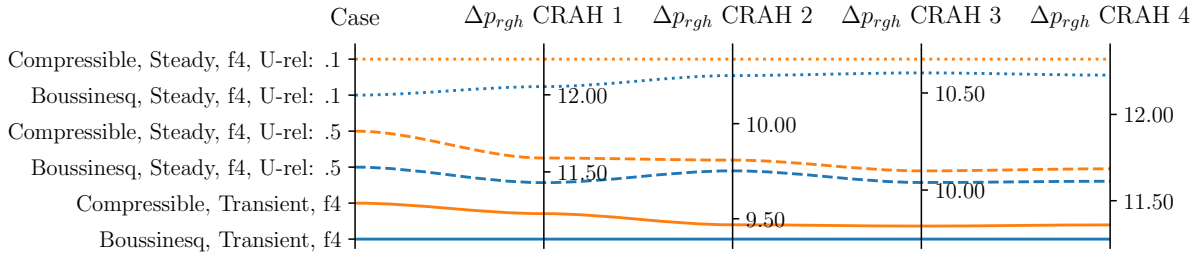

Figure 8. Mean pressure drop in Pa per cooling unit for two steady solutions using different under relaxation factors (0.1 and 0.5) for the velocity and one transient case

Evaluation of solvers and a steady steate assumption for the *Reduced* flow rate case.

Higher Ri (increased buoyant convection) results in return temperatures on the CRAH-units matching within 0.1 K for the finest grid for both the steady and transient solutions. For this case, Fig. 9 shows how the pressure drops match between the solution types and is consistent across the solvers.

The increased pressure drop resolved for the *forced* compressible case in comparison to the incompressible case is not here seen for the *reduced* case. It is rather the opposite, meaning a marginally lower pressure drop is observed when compressibility is introduced. This is possibly an effect introduced by natural convection, where the pressure drops are less attributed to flow separation and resolved natural convection aids the rising of hot air. The effect of solver on the pressure drop is seen to be in the range of 0.1 Pa, which for this case is significant. The numerical artifacts by introducing a steady solution here give a negligible added pressure drop shown as the dashed line in Fig. 9.

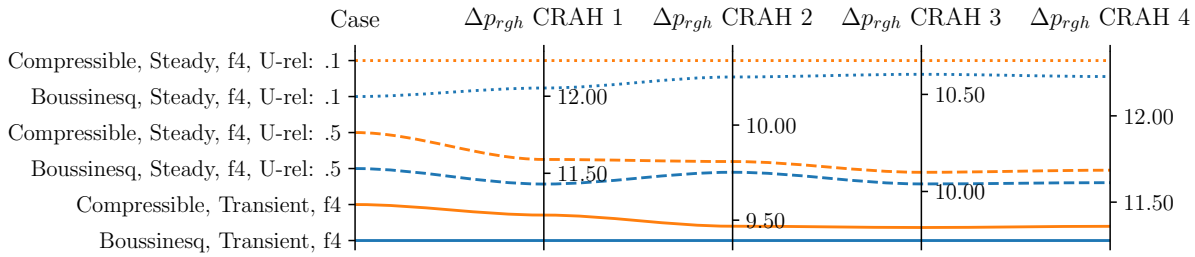

Figure 9. CRAH-unit pressure drops in Pa, steady and transient results

3.3. **Comparison between the typical and reduced case.** Figures 10, 11 and 12 show a cross section (same as in Fig. 2) of the compressible "f4" solutions, with mean values of velocity magnitude, turbulent kinetic energy, and temperatures sampled for 5 minutes modelled flow time. The turbulent kinetic energy is seen to be more prominent in the *typical* case, along with the velocity magnitudes. These quantities take on their largest values near the jet-like flow coming from rack 2 and near the outlets.

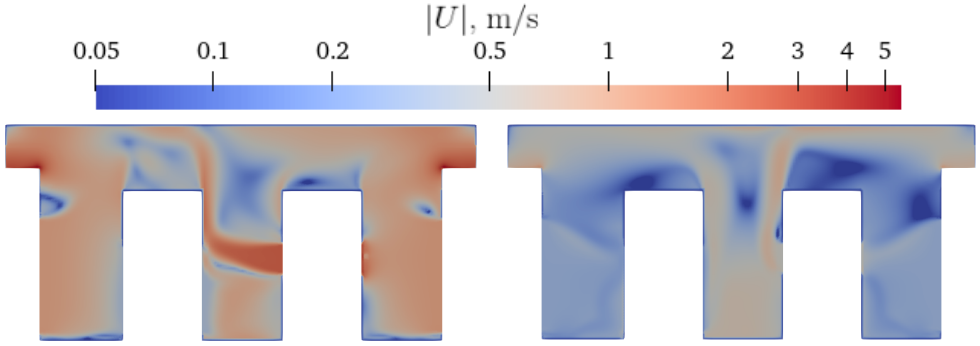

(a) Typical case **(b)** Reduced case

Figure 10. Time averaged velocity magnitude, $|U|$ in m/s for the cross section

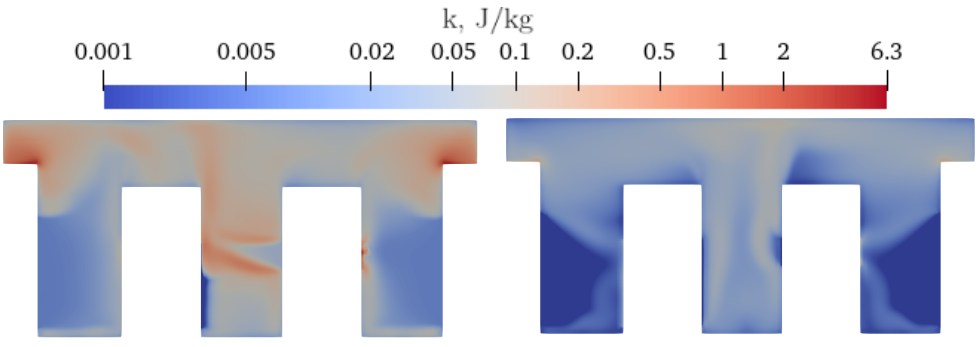

(a) Typical case **(b)** Reduced case

Figure 11. Time averaged turbulent kinetic energy for the cross section

Density differences measured in the compressible solver are approximately 4% and 25% for the *typical* and *reduced* case respectively. The natural convection occuring in the *reduced* case is demonstrated by the column of higher temperature air rising as seen in Fig. 12. Lower estimated bounds for the turbulent eddy viscosity of 0.01 J/kg and 0.004 J/kg in the resolved turbulent flow for the two cases give eddy viscosity ratios (ν_t/ν) above 660 and 260 respectively for the two cases. A typical ratio that describes fully turbulent flow is around 100, so the k-epsilon model can in this view be considered applicable [19].

In light of a Ri based on the same β and height (1 m) as in the introduction, velocity values were obtained to be in the span of $u \in (0.14, 1.83)$ m/s. These velocities correspond well with the limits of forced to mixed convection and from mixed to natural convection respectively as mentioned. Evaluating the temperatures near the roof in Fig. 12 along with the volume weighted velocities, estimates of Ri in

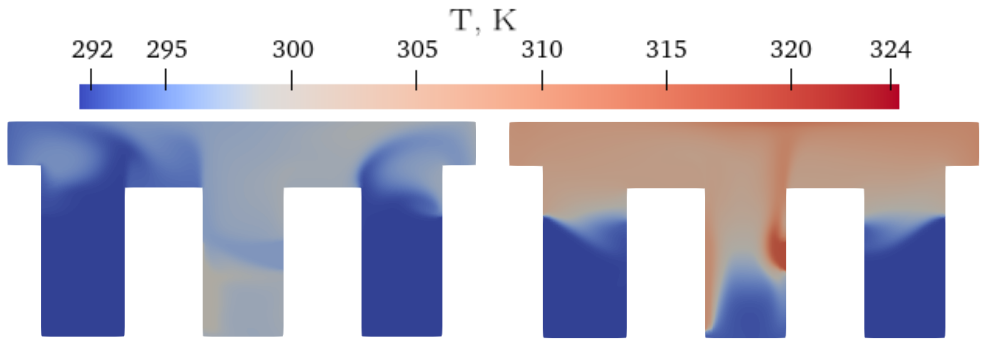

(a) Typical case **(b)** Reduced case

Figure 12. Time averaged temperature for the cross section

the domain can be made that relate to the nature of the flow and possible stratification. Expectation values for the domain velocities are 0.60 m/s and 0.21 m/s with roof temperatures estimated as 300 K and 310 K for the typical and reduced cases respectively(based on the compressible model). Using the supply temperature of 291.45 K a Ri is obtained as $\mathrm{Ri}_{\mathrm{typical}} = 0.8$ and $\mathrm{Ri}_{\mathrm{reduced}} = 14.1$ ergo both cases are within the regime of mixed convection, $Ri \in (0.3, 16)$. It is seen that an expected Ri for the two cases become close to the reference literature values for pure forced and natural convection, respectively when applying the above specified height.

Solver times for the finest compressible case is about 22% and 15% faster than the Boussinesq solver for the *typical* and *reduced* cases respectively. This is explained by an increased number of pressure iterations per inner time step loop exhibited by the Boussinesq solver, being nearly five times as many as for the compressible solver. This is believed to be a consequence of the nature of the boundary conditions. The incompressible solver is expected to perform better for cases where there are more boundary conditions directly specifying a pressure, other than the single pressure reference boundary that is employed in these simulations. The incompressible solver is therefore expected to work faster when there are multiple pressure boundaries acting as reference areas, reducing the numerical stiffness of the model.

Transient development of the temperatures at the CRAH-return areas along with rack 1 is presented in Fig. 13. This rack is included as it indicates a slight recirculation of heated air. The development timescales of return temperatures are seen to be similar for both cases. It is noteworthy that the *typical* case shows a periodic variation in temperature for two of the CRAH-return areas, likely being a consequence of flow separation.

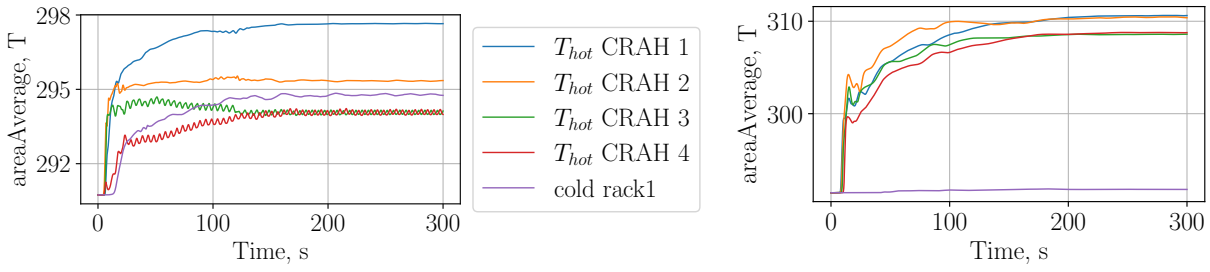

(a) Typical case **(b)** Reduced case

Figure 13. Settling of CRAH return temperatures for the finest grid

Fig. 14 shows a significant difference in temperature distribution by height between the different Ri, with the scale chosen such that light blue interval represents the intermediate range of mixed temperatures. This range is 293-297 K for the *typical* case and 294-305 K for the *reduced* case and the sum of the bars equal the entire volume of the data center. The high Ri case shows significant stratification of high temperatures of which features can also be identified in Fig. 12. The typical convection case shows no hint of this type of stratification.

Fig. 15 shows how the finest grid solutions compared for the two solvers and cases match. No significant difference between the temperature distributions for the solvers can be identified.

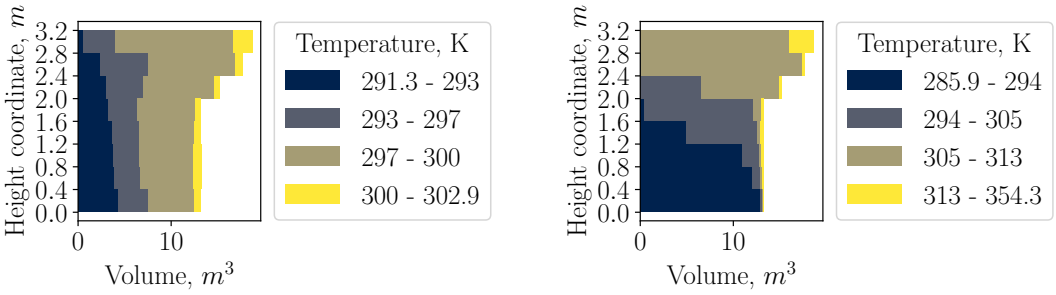

(a) Typical case **(b)** Reduced case

Figure 14. Cumulative temperature histograms by height for both cases. Based on the compressible solution at finest grid

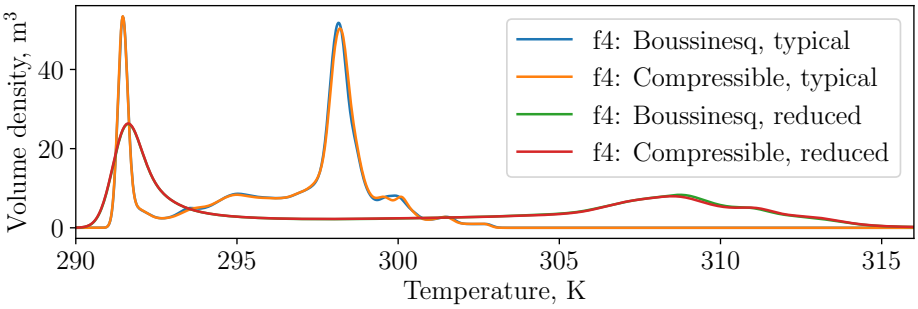

Figure 15. Temperature distributions for the cases solved at the finest grid

Discussion & Conclusions

The Boussinesq and compressible solvers in OpenFOAM® for convective heat transfer are both viable options for temperature ranges that apply to data center ventilation applications. The compressible solver provide faster convergence for the simulations done here and has indication to also be slightly more accurate at coarser grids. This is believed to be case specific due to how the boundary conditions impose a fixed flow rate at all inlet/outlet boundaries with the pressure reference opening as an exception. For running parametric studies of data center fluid flow, it can be concluded that one single grid sizing might not be enough to correctly do the wall modelling nor reduce thermal diffusion for different flow rates.

KDE distibutions can indicate how much volume contains mixed hot and cold air, though not whether there is active mixing or if there are local hot-spots or direct hot air recirculation to racks. Here the distributions are useful as a tool to indicate the quality of the resolved flow with respect to numerical diffusion. Air flow of higher velocity may mix a lot more hot and cold air than natural convection per unit time. To enable quality CFD research on the amount of lost energy in mixing, numerical effects on temperature diffusion needs to be at a minimum.

Both the PISO and PIMPLE methods for time iteration were tested and are viable options, depending on the stability of PIMPLE at the chosen time step. In terms of computational economy and accuracy, this type of simulations can benefit from a larger time step enabled by an implicit pressure-velocity coupling. The pressure drop is shown to be dependent on relaxation factors for the steady solutions of the *typical* case (lower Ri). Transient cases thus provide better value in terms of studying the statistics on the mixing of hot and cold air where Ri is low. An issue here is that he time step needs to be small for the OpenFOAM® solution to converge, such that it begins to match the turbulent time-scales. This is less than ideal for any applied unsteady RANS model.

Pressure drops are consistently higher using the compressible solver for the *typical* case and reversed trends are seen for the *reduced* case. To reduce numerical diffusion and at the same time meet requirements for wall function y^+ puts high demands on the grid to enable a solution in the asymptotic range. To produce qualitative CFD solutions for different flow rates and Ri therefore require grids that fulfil these

criteria. For the simulations done in this work, the f_2 grid is considered sufficient, utilizing a reference cell size of 60 mm.

Although a fraction of the *typical* case flowrate is used for the *reduced* case to obtain higher grade heat in a semi-realistic setting, not more than a half might be applicable. The flow rates used affect the solution time of the solver as well, such that the higher Ri case makes for significantly faster solver times. The *reduced* case (higher Ri) also increases the feasability to use a steady solution at little cost of solution accuracy.

4. Acknowledgements

The authors would like to acknowledge RISE - ICE Data center for support in configuring and maintaining cluster resources for distributed computing.

Author Contributions: Conceptualization, H.B., A.-L.L., T.S.L.; methodology, H.B.; software, H.B.; validation, H.B.; formal analysis, H.B., A.-L.L.; investigation, H.B.; resources, H.B.; data curation, H.B.; writing—original draft preparation, H.B.; writing—review and editing, A.-L.L., T.S.L.; visualisation, H.B.; supervision, A.-L.L.; project administration, A.-L.L.; funding acquisition, A.-L.L. All authors have read and agreed to the published version of the manuscript

4.1. **Funding:** This study was supported by the Swedish Energy Agency under grant 43090-2, Cloudberry Data centers.

4.2. **Conflicts of interest:** The authors declare no conflict of interest

References

[1] H. M. Ljungqvist, L. Mattsson, M. Risberg, and M. Vesterlund, "Data center heated greenhouses, a matter for enhanced food self-sufficiency in sub-arctic regions," *Energy*, vol. 215, p. 119169, 2021.
[2] S. V. Patankar, "Airflow and cooling in a data center," *Journal of Heat transfer*, vol. 132, no. 7, p. 073001, 2010.
[3] J. Ni and X. Bai, "A review of air conditioning energy performance in data centers," *Renewable and sustainable energy reviews*, vol. 67, pp. 625–640, 2017.
[4] J. Sjölund, M. Vesterlund, N. Delbosc, A. Khan, and J. Summers, "Validated thermal air management simulations of data centers using remote graphics processing units," in *IECON 2018-44th Annual Conference of the IEEE Industrial Electronics Society*. IEEE, 2018, pp. 4920–4925.
[5] J. H. Ferziger and M. Perić, *Computational methods for fluid dynamics*. Springer, 2020, vol. 4.
[6] J. Sarkinen, R. Brännvall, J. Gustafsson, and J. Summers, "Experimental analysis of server fan control strategies for improved data center air-based thermal management," in *2020 19th IEEE Intersociety Conference on Thermal and Thermomechanical Phenomena in Electronic Systems (ITherm)*. IEEE, 2020, pp. 341–349.
[7] D. J. Tritton, *Physical fluid dynamics*. Springer Science & Business Media, 2012.
[8] E. Sparrow, R. Eichhorn, and J. Gregg, "Combined forced and free convection in a boundary layer flow," *The Physics of Fluids*, vol. 2, no. 3, pp. 319–328, 1959.
[9] A. Limane, H. Fellouah, and N. Galanis, "Thermo-ventilation study by openfoam of the airflow in a cavity with heated floor," in *Building Simulation*, vol. 8, no. 3. Springer, 2015, pp. 271–283.
[10] J. Summers, N. Kapur, and H. Thompson, "Design of data centre rack arrangements using open source software," in *Semiconductor Thermal Measurement and Management Symposium (SEMI-THERM), 2013 29th Annual IEEE*. IEEE, 2013, pp. 45–51.
[11] E. Wibron, A.-L. Ljung, and T. S. Lundström, "Comparing performance metrics of partial aisle containments in hard floor and raised floor data centers using cfd," *Energies*, vol. 12, no. 8, p. 1473, 2019.
[12] E. Wibron, A.-L. Ljung, and T. S. Lundström, "Computational fluid dynamics modeling and validating experiments of airflow in a data center," *Energies*, vol. 11, no. 3, p. 644, 2018.
[13] X. S. Zhang, "Coarse-grid cfd: The effect of grid size on data center modeling," *ASHRAE Transactions*, vol. 114, p. 166, 2008.
[14] P. J. Roache, "Quantification of uncertainty in computational fluid dynamics," *Annual review of fluid Mechanics*, vol. 29, no. 1, pp. 123–160, 1997.
[15] W. A. Abdelmaksoud, H. E. Khalifa, T. Q. Dang, R. R. Schmidt, and M. Iyengar, "Improved cfd modeling of a small data center test cell," in *Thermal and Thermomechanical Phenomena in Electronic Systems (ITherm), 2010 12th IEEE Intersociety Conference on*. IEEE, 2010, pp. 1–9.
[16] S. Patankar, *Numerical heat transfer and fluid flow*. CRC press, 2018.
[17] J. P. Van Doormaal and G. D. Raithby, "Enhancements of the simple method for predicting incompressible fluid flows," *Numerical heat transfer*, vol. 7, no. 2, pp. 147–163, 1984.
[18] D. W. Scott, *Multivariate density estimation: theory, practice, and visualization*. John Wiley & Sons, 2015.
[19] C. Rumsey. (2021) Nasa, turbulence modeling resource. [Online]. Available: https://turbmodels.larc.nasa.gov/index.html